Presented at the Second International Symposium on Land Subsidence, Anaheim, CA, December 10-17, 1976

LBL-4462
c.1

Energy and Environment Division

Numerical Simulation of Reservoir Compaction in Liquid Dominated Geothermal Systems

M. J. Lippmann, T. N. Narasimhan and P. A. Witherspoon

December 1976

Lawrence Berkeley Laboratory University of California/Berkeley

Prepared for the U.S. Energy Research and Development Administration under Contract No. W-7405-ENG-48

LBL-4462
c.1

NUMERICAL SIMULATION OF RESERVOIR COMPACTION IN LIQUID DOMINATED GEOTHERMAL SYSTEMS

by

M. J. Lippmann, T. N. Narasimhan and P. A. Witherspoon
Lawrence Berkeley Laboratory
University of California
Berkeley, California 94720

December 1976

Presented at the
Second International Symposium on Land Subsidence
Anaheim, California, December 10-17, 1976

This work was supported in part by the U. S. Energy Research and Development Administration

NUMERICAL SIMULATION OF RESERVOIR COMPACTION IN LIQUID DOMINATED GEOTHERMAL SYSTEMS

Marcelo J. Lippmann, T. N. Narasimhan and P. A. Witherspoon
Lawrence Berkeley Laboratory
University of California
Berkeley, California 94720

Abstract

Recently much attention has been focused on the development of geothermal systems. A large number of geothermal fields are of the hot water type, dominated by circulating liquid that transfers most of the heat and largely controls subsurface pressures. During the exploitation of such systems, a reduction of pressures is inevitable which, in some areas may lead to land subsidence.

A numerical model is introduced which simulates the effects of fluid production as well as reinjection on the vertical deformation of water dominated geothermal reservoirs. This program, based on an Integrated Finite Difference technique and Terzaghi's one-dimensional consolidation model, computes the transport of heat and water through porous media, and resulting pore volume changes. Examples are presented to show the effects of reservoir heterogeneities on the compaction of these hot water systems, as well as the effects of different production-injection schemes. The use of isothermal models to simulate the deformation of non-isothermal systems is also investigated.

Introduction

The production of fluids from geothermal systems may result in ground surface displacements due to the lowering of pressures in the reservoir and surrounding rocks. These displacements may not only affect installations directly related to the geothermal field (e.g., well casings, steam transmission lines, power plant) but also nearby roads, buildings, and irrigation canals. Therefore it is important to foresee the magnitude and location of the so-called "subsidence bowl" as soon as adequate data on the geologic structure, stratigraphy, rock properties, and proposed development program become available. A number of models to simulate the vertical and horizontal ground deformations in geothermal systems have been or are being developed. These are reviewed in another paper presented at this meeting (Finnemore and Gillam, 1976).

Here, we introduce a mathematical model to simulate the transport of heat and water through a porous geothermal system, including the vertical deformations produced by effective stress changes. This code named "CCC" (for Conduction-Convection-Consolidation) is restricted to one-phase water dominated geothermal fields. At the present time, these systems have the largest potential for developing geothermal energy for electrical and non-electrical uses. They are characterized by circulating liquid that transfers most of the heat and largely controls subsurface pressures (Renner, et al., 1975).

A number of examples are presented below to illustrate some of the capabilities of our computer program. We shall demonstrate the effect of geologic heterogeneities on the behavior of the geothermal system as well as the effect of the location of production and injection wells. A comparison of results will also be made when the system is analyzed under isothermal and non-isothermal conditions.

Method and Governing Equations

Program CCC is based on the numerical models SCHAFF (Sorey, 1975) for

mass and heat transport through saturated porous media, and TRUST (Narasimhan, 1975) for one-dimensional isothermal consolidation. The code can simulate one, two or three-dimensional, heterogeneous, isotropic, non-isothermal systems. Deformation parameters may be non-linear and non-elastic; the thermal and hydraulic properties can be temperature and/or pressure dependent.

An integrated finite difference method (Narasimhan and Witherspoon, 1976) is used to solve the energy and fluid flow equations. In integral form the flow equation for a slightly compressible fluid (e.g., water) is given by:

$$\frac{\partial}{\partial t}\int_V \frac{\rho}{1+e}\left(e\kappa + \frac{de}{d\sigma'}\right) P\,dV = \int_S \frac{k\rho}{\mu}(\nabla P - \rho\bar{g})\cdot\bar{n}\,dS + \int_V Q\,dV \qquad (1)$$

and the energy equation is given by:

$$\frac{\partial}{\partial t}\int_V (\rho c)_M T\,dV = \int_S K_M \nabla T\cdot\bar{n}\,dS - \int_S \rho c_F \delta T \bar{v}_d\cdot\bar{n}\,dS + \int_V q\,dV \qquad (2)$$

where, t is time, ρ fluid density, e void ratio, κ fluid compressibility, σ' effective stress, P pore pressure, V volume, k intrinsic permeability, μ viscosity, $\bar{g}$ gravitational acceleration, $\bar{n}$ outward unit normal on surface S, Q mass injection rate per unit volume, $(\rho c)_M$ heat capacity per unit volume of the solid-fluid mixture, K_M thermal conductivity of the solid-fluid mixture, c_F fluid specific heat capacity at constant volume, δT difference between the mean temperature within the volume element and that on the surface element dS, $\bar{v}_d$ Darcy velocity, and q heat injection rate per unit volume. Details of the method used to solve these equations are given by Sorey (1975) and Narasimhan (1975), and will not be repeated here.

Concurrent with the mass and energy flow, the vertical deformation of the geothermal system is simulated based on the one-dimensional consolidation theory of Terzaghi. The void ratio at each nodal point is computed by using "e-log σ'" curves (Figure 1). According to the preconsolidation and effective stresses at the point, the program calculates the void ratio by using either the virgin curve (of slope C_c) or swelling-recompression curves (of slope C_s). The model neglects the hysteresis between swelling and recompression curves. While the pore volume changes with effective stress, the solid volume is defined to remain constant; the thermal expansion of the rock skeleton is not considered. Because of

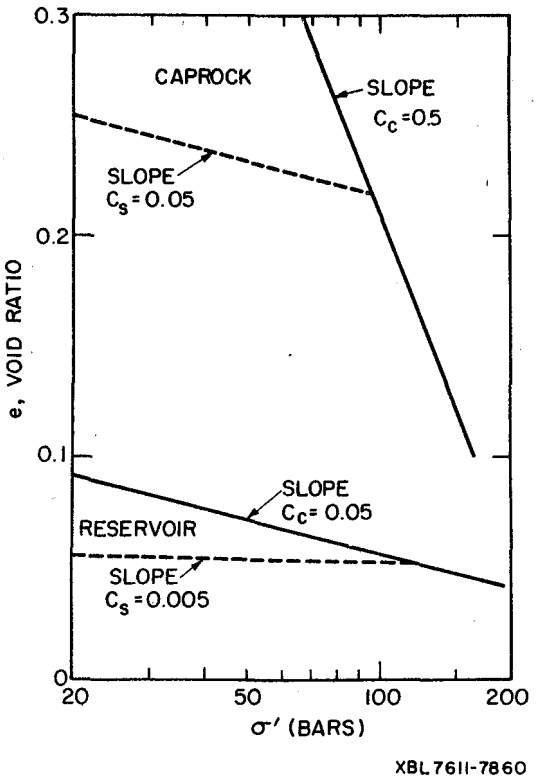

Figure 1. Plot of void ratio (e) versus effective stress (σ') for caprock and reservoir of example 4.

the one-dimensional nature of the consolidation model the pore volume changes caused by void ratio changes are directly reflected in a vertical deformation of the individual volumetric nodes.

The deformations computed by this model are restricted to those of the reservoir and neighboring saturated formations which release water from storage to partly or wholly compensate for the fluid withdrawn. These vertical displacements may or may not be directly expressed at the ground surface. The external loading of the overburden, caused by the vertical deformation of the deeper geothermal system, may result in displacements at the surface that may be different in magnitude and direction. Future versions of this model will include the computation of vertical and horizontal displacements at the ground surface itself.

The flow and energy equations (1) and (2) are interconnected by (a) the second order equation of state for the fluid,

$$\rho = \rho_o[1 - \beta(T-T_o) - \gamma(T-T_o)^2] \qquad (3)$$

where, β and γ are coefficients of thermal expansion, and ρ_o and T_o are the reference density and temperature, respectively, for the fluid, (b) the Darcy velocity used in the convection term of the energy equation, and (c) the temperature and/or pressure dependence of certain parameters.

Because these interrelations, equations 1 and 2 are solved alternatively by interlacing their solutions in time; this is shown schematically on Figure 2. The flow equation solves for P, $\bar{v}_d$ and e assuming that the temperature dependent properties of the fluid and rock remain constant. Then, the energy equation is used to obtain T assuming that $\bar{v}_d$ and pressure dependent properties remain constant. Since the temperature varies much more slowly than the pressure, much smaller time steps have to be taken in the flow cycles than in the energy cycles (Figure 2) in order to compute pressure variations accurately.

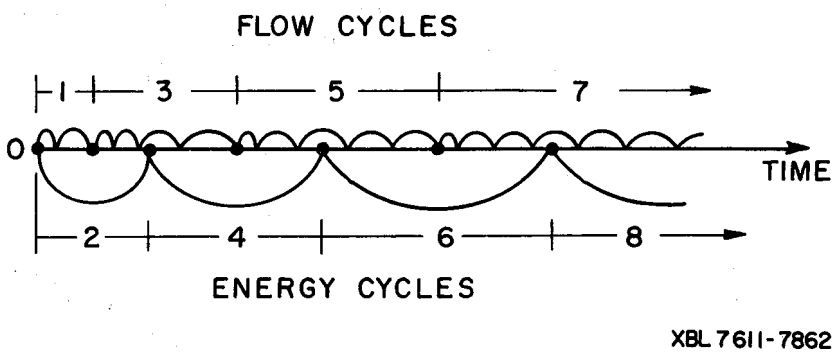

Figure 2. Interlacing of flow and energy calculations

Examples and Results

Four examples are presented below. In all cases it is assumed that, (a) the systems are normally consolidated (i.e., initial effective stresses and preconsolidation stresses are equal), (b) total stresses do not change in time, and (c) the intrinsic permeability (k), thermal conductivity (K_M), and heat capacity of the rock (c_R), as well as the compressibility (κ) and coefficients of thermal expansion (β,γ) of the water are constant. These assumptions are made to simplify the examples presented here, although the program can consider more complex conditions and relationships. The fluid density (ρ), heat capacity (c_F) and viscosity (μ) are temperature dependent, while the void ratio (e) is dependent on pore pressure and previous stress history.

Example 1. System with caprock of variable thickness

This case shows a totally penetrating well placed at the center of an axisymmetric system which has a caprock of variable thickness. The well withdraws 2.8 x 10^6 kg/day of water uniformly along the thickness of the reservoir. Figure 3 shows the dimensions, boundary conditions and initial temperature distribution for this system. At t = 0, only heat conduction occurs between the boundaries, since the Rayleigh number (Ra) in the reservoir is less than 20. This dimensionless number is equal to the ratio between the buoyant and viscous forces acting in the reservoir, and at this low Ra, free convection is not expected to occur.

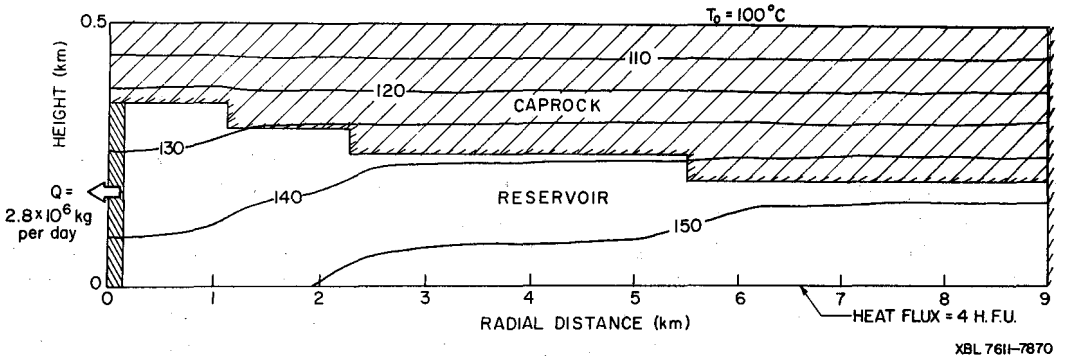

Figure 3. Example 1. Geometry, initial temperature and boundary conditions

The shape of the initial isotherms reflects the non-uniform thicknesses of materials of different thermal conductivities under the prevailing boundary conditions. The lower boundary is impermeable with a constant influx of 4 x 10^{-6} cal cm^{-2} sec^{-1} (4 H.F.U.). The upper boundary is isothermal (100°C) and impermeable. The outer radial boundary is closed both to heat and fluid flow. The overburden (not shown) is 1000 m thick and its average density is 2.5 g cm^{-3}. The rock and fluid properties used in this example are given in Tables 1 and 2.

When production starts, water in the reservoir flows essentially radially towards the well and vertically downward in the caprock. The resulting consolidation after 2400 days is shown on Figure 4. Near the well a maximum compaction of 29.2 cm was determined, of which about 70% occurred in the caprock.

The same system was also investigated under isothermal

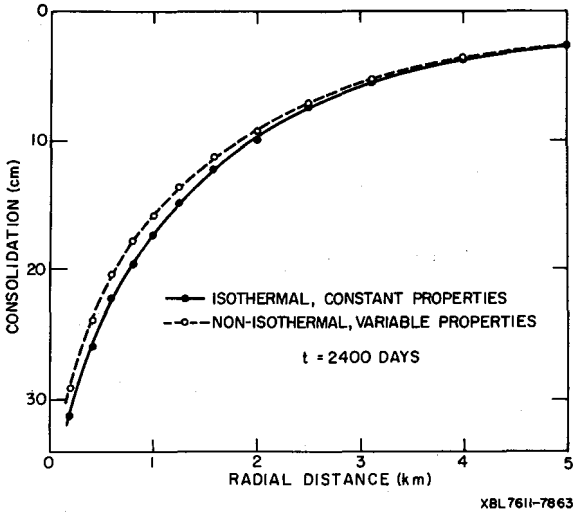

Figure 4. Example 1. Consolidation versus distance under isothermal and non-isothermal conditions.

Table 1. Material properties of rocks used in examples 1 to 3

	Caprock	Reservoir
Thermal conductivity (K_M) (mcal cm^{-1} sec^{-1} $°C^{-1}$)	2.52	6.64
Rock heat capacity (c_R) (cal g^{-1} $°C^{-1}$)	0.222	0.232
Rock density (ρ_R) (g cm^{-3})	2.70	2.65
Intrinsic permeability (k) (cm^2)	1×10^{-12}	5×10^{-10}
Reference void ratio (e_o)	0.250	0.053
Reference effective stress (σ'_o) (bars)	185	185
Slope of virgin curve (C_c)	0.5	0.05
Slope of swelling-recompression curve (C_s)	0.05	0.005

Table 2. Fluid properties of water used in all examples

Compressibility (κ)	5.5×10^{-5} $bars^{-1}$
Coefficient of thermal expansion (β)	3.17×10^{-4} $°C^{-1}$
Coefficient of thermal expansion (γ)	2.56×10^{-6} $°C^{-2}$
Reference temperature (T_o)	25°C
Reference density (ρ_o)	0.997 g cm^{-3}
Viscosity (μ) and heat capacity (c_F)	f(T) for P = 100 bars

conditions using fluid properties corresponding to 135°C, which is the average temperature for example 1. In this case, the consolidation within 2 km from the well was between 7 and 9% larger than under non-isothermal conditions (Figure 4). The larger computed compaction for the isothermal case is apparently to be attributed to the viscosity effects; in the isothermal system a constant viscosity of 0.284 cp was used, whereas in the non-isothermal case the viscosity varied between 0.202 cp and 0.315 cp across the system.

From this example, we conclude that in order to use an isothermal model to simulate the behavior of a non-isothermal system, periodic adjustments of model properties may have to be made to account for the temperature variations that can occur as the simulation progresses in time.

Example 2. System with low permeability lens in reservoir

The system considered here differs from that of example 1 in that a lens of the same material as the caprock has been incorporated into the reservoir. This lens increases the tortuosity of the flow lines, resulting in more pressure drop near the well and less drop further away. This is shown on Figure 5 where lines of equal pressure reduction at t=2400 days are plotted for examples 1 and 2. The effects of these differences in pore pressure change produce different consolidation patterns as shown on Figure 6. These results indicate that it is possible to have a larger compaction away from the producing well due to a heterogeneity in the

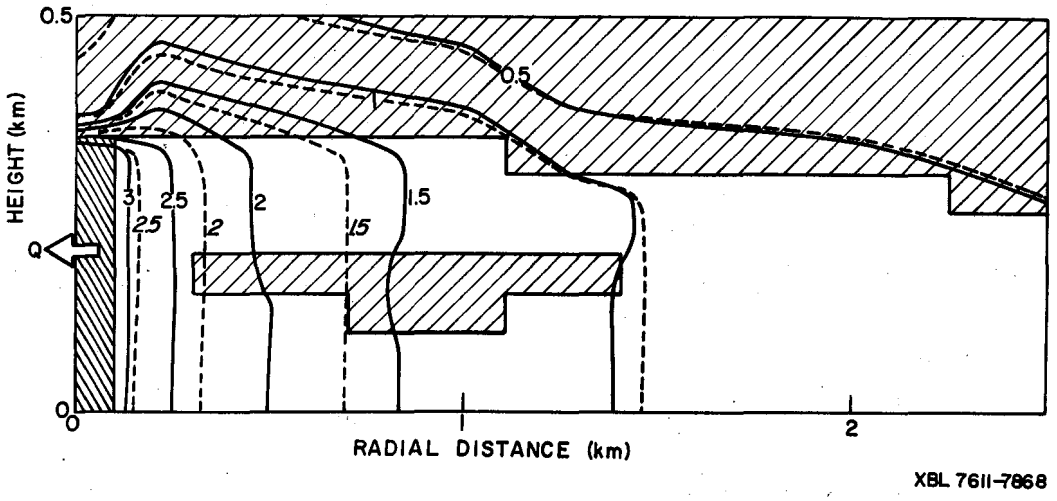

Figure 5. Pore pressure drop, in bars, after 2400 days of water withdrawal. Dashed lines: Example 1 (without lens); Solid lines: Example 2 (with lens).

reservoir. The lens provides a larger volume of more compressible material at locations where large pressure changes are occurring.

This type of heterogeneity in the reservoir could explain why in the Wairakei geothermal field of New Zealand, the maximum ground displacements occur in an area distant from the more intensively developed well field (Stillwell et al., 1976). This idea needs further investigation using three dimensional systems with non-uniform caprocks and differently shaped lenticular structures.

Example 3. System with intercalated layer in reservoir

This example is intended to show that even when all the produced water is reinjected, some amount of compaction cannot be avoided. The geometry, properties, initial and boundary conditions used here are similar to those of example 1. A layer of the same material as the caprock is intercalated in the reservoir as shown in Figure 7. The layer might be an aquitard partially dividing the reservoir in two parts. The separation is

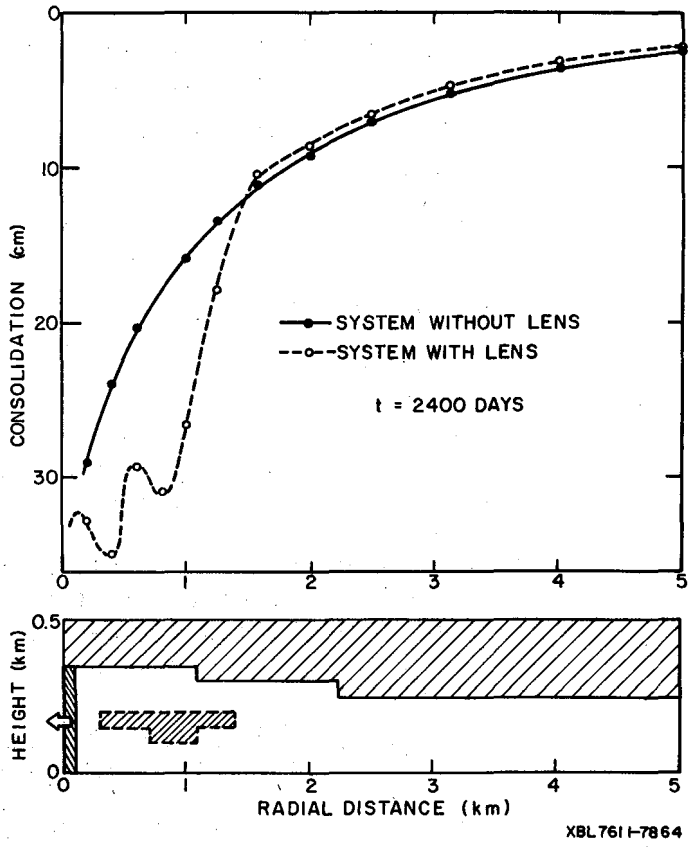

Figure 6. Consolidation versus distance after 2400 days of water withdrawal. Solid lines: Example 1; Dashed lines: Example 2

not complete since the layer only extends radially 1750 m from the well. A production rate of 1.2 x 10^6 kg/day of hot water is maintained from the upper 150 m of the reservoir. The same mass is reinjected into the lower 100 m of the reservoir, but the temperature of the injected water is only 25°C. The total pressure changes after 15 years of simulation time are shown in Figure 8. Note that pressures decrease in the upper part and increase in the lower part. As shown in Figure 7, the consolidation of the system is restricted to the first 1500 m out from the well. Negligible effects occurred beyond this distance from the well which agrees with the location of the curve for zero pressure change (see Figure 8). The development of consolidation with time is depicted on Figure 7. At the beginning, the compaction rate of the system is significant, but it falls off rapidly with time.

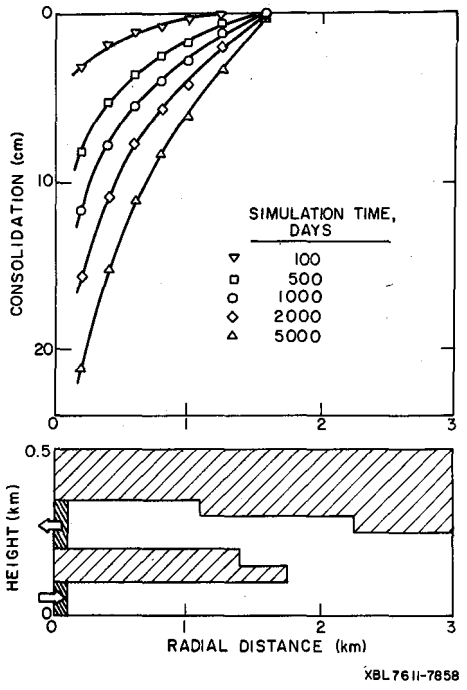

Figure 7. Example 3. Geometry and consolidation versus time and distance.

Because of the injection of colder waters, the lower part of the reservoir slowly cools. After 15 years, the thermal front separating the colder and warmer waters is located at a radial distance of about 175 m from the well. The hydrodynamic front, indicating the position of the reinjected water which largely has been warmed up by the heat stored in the reservoir rock skeleton, has advanced to about 650 m from the well. The approximate location of the hydrodynamic front has been calculated by assuming that the water has flowed only radially away from the injection well. This is only a simplification since some of the water actually has seeped upward through the layer separating the reservoir.

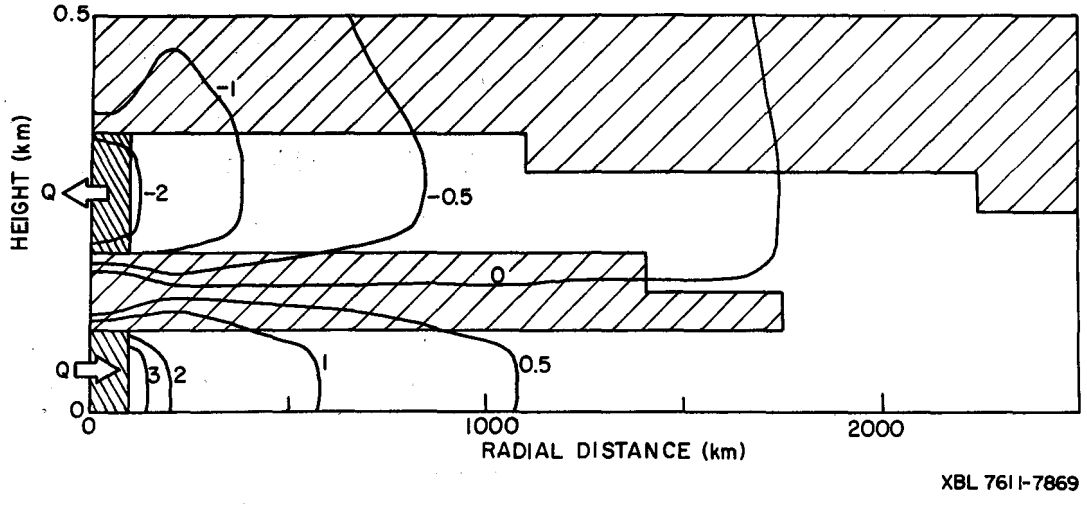

Figure 8. Example 3. Pressure changes, in bars, after 15 years of simulation.

Due to the colder temperature near the well and the higher mass flow rate per unit injected area of the well, large increases of pressure occur in the lower part of the reservoir, which are greater in magnitude than the pressure reductions in the upper reservoir. Even under these conditions, a net compaction still occurs around the well. This suggests that it may be necessary to have rates of reinjection that are larger than the production rates in order to minimize the effects of consolidation. Further work along these lines is needed.

Example 4. Convecting system with three layers

This last example is intended to describe the response of a free convecting system to two different production and reinjection schemes. The system is a parallelepiped 550 m high, 750 m wide and 50 m deep and contains three different layers (Figure 9). The caprock and reservoir are deformable, their "e-log σ'" curves are given in Figure 1, but the baserock is incompressible. Tables 2 and 3 list the fluid and material properties used in this example. Because of the large temperature difference between the top and bottom boundaries (260°C), the heat flow across this system is much larger than in the previous cases. It is approximately 37 H.F.U. The Rayleigh number for the reservoir is about 93, which exceeds the critical Ra ≈ 40. Indeed, free convection is established in the reservoir as is shown schematically in Figure 9 by the dashed circles and reflected by the shapes of the isotherms. Two production-injection schemes were considered. In both cases a total of 4 x 10^4 kg/day of water were produced and 3.2 x 10^4 kg/day of 100°C water were reinjected

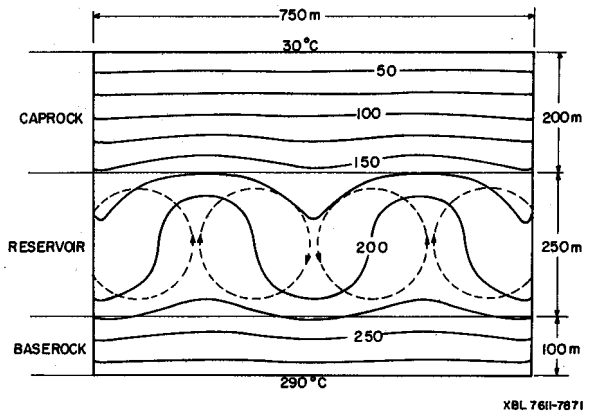

Figure 9. Example 4. Geometry and initial temperature distribution. Dashed circles: Convection cells (schematic representation).

Table 3. Material properties of rocks used in example 4

	Caprock	Reservoir	Baserock
Thermal conductivity (K_M) (mcal cm^{-1} $sec^{-1}°C^{-1}$)	4.98	4.98	5.53
Rock heat capacity (c_R) (cal $g^{-1}°C^{-1}$)	0.222	0.232	0.222
Rock density (ρ_R) (g cm^{-3})	2.70	2.65	2.70
Intrinsic permeability (k) (cm^2)	1 x 10^{-12}	5 x 10^{-10}	1 x 10^{-13}

(80% reinjection). The amount of water involved is rather small, and the rates used in this example were such as to avoid "overpowering" the natural convection cells, each of which transported about 7000 kg/day of water through the system. In the first case (example 4a) water is removed at the top of the ascending columns of convection and injection is at the bottom of the descending columns (Figure 10A). In example 4b water is removed at the bottom of the ascending columns and injection is at the top of the descending columns (Figure 11A). A symmetrical arrangement of sources and sinks was used to retain the symmetry implied by the impermeable side boundaries.

Figures 10B and 11B show the resulting temperature distribution for both cases after 20 years of simulation. A general cooling of the system is observed. There was no significant difference in the amount of consolidation occurring in either case. A difference might possibly be detected after longer period of time because the cooling patterns are not the same in both cases. The consolidation is fairly uniform across the system being slightly larger (2%) over the pumping areas. Figure 12 shows the development of consolidation in time for example 4a. The compaction increases almost linearly with time, and the contribution of the reservoir to the total consolidation is important only at early time. Later, most of the compaction occurs in the caprock. This may be explained by the delayed lowering of pore pressure in the caprock (see Figure 13).

For comparison purposes, example 4a was also modelled as a 175°C isothermal system. Pore pressures, total and preconsolidation stresses were the same. The resulting compaction was 4-6% higher than that of the non-isothermal case. When pressure changes are compared (Figure 14), it is evident that in the isothermal system, the pore pressure decreased more in the upper part of the caprock and less in the lower part as well as in the reservoir.

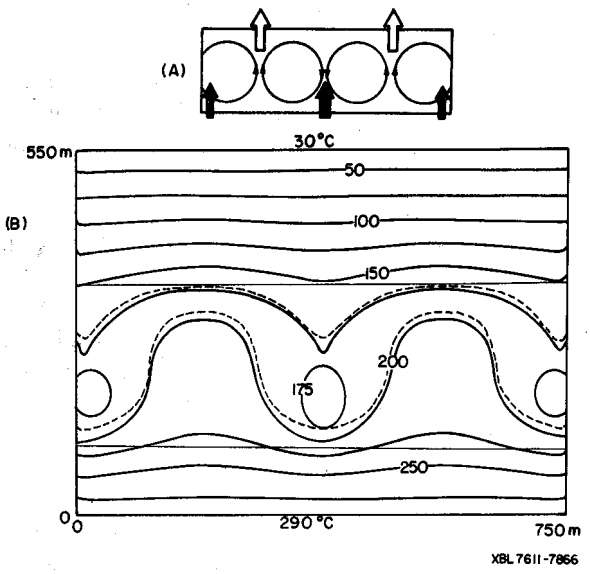

Figure 10. Example 4a. (A) Dark arrows: injection; light arrows: production. (B) Temperature distribution after 20 years of simulation. Dashed lines: initial 175° and 200°C isotherms.

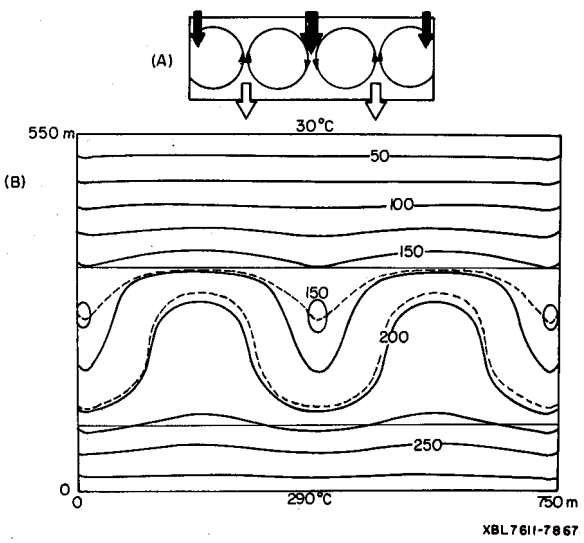

Figure 11. Example 4b. (A) Dark arrows: injection; light arrows: production. (B) Temperature distribution after 20 years of simulation. Dashed lines: initial 175° and 200°C isotherms.

As in example 1, the unequal response to the withdrawal of fluids can be attributed to the viscosity differences in the two cases. In the isothermal system, the viscosity is uniform (0.212 cp), but in the non-isothermal case it varies from 0.150 cp at the bottom of the reservoir, to 0.446 cp at the top of caprock. The differences in the distribution of fluid density in the isothermal and non-isothermal cases will also have similar effects on pressure distribution and compaction as the viscosity variation, but the magnitudes will be smaller relative to viscosity effects.

The final example suggests that compaction of water dominated geothermal fields with large temperature differences and complex fluid patterns will be difficult to model as isothermal systems. This is especially the case if one is interested in the pressure and compaction history at particular parts of the system.

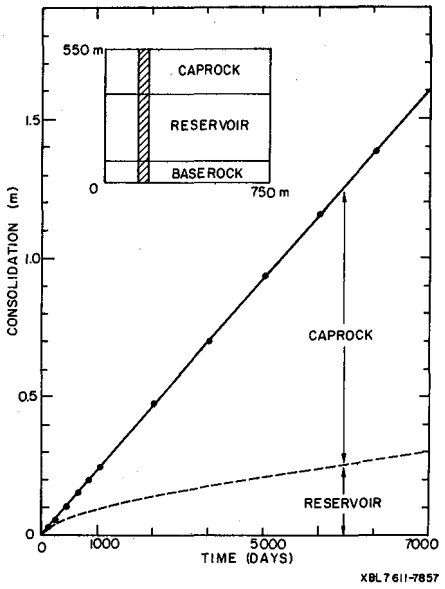

Figure 12. Example 4a. Consolidation versus time (corresponds to the column indicated in the insert).

References

Finnemore, E. J. and M. L. Gillam, 1976. Compaction processes and mathematical models of land subsidence in geothermal areas: Proc. 2nd Int. Symp. Land Subsidence, Anaheim, Ca., Dec. 13-17, 1976.

Narasimhan, T. N., 1975. A unified numerical model for saturated -unsaturated groundwater flow: Ph.D. thesis, Univ. California, Berkeley, 244 p.

Narasimhan, T. N. and P. A. Witherspoon, 1976, An integrated finite difference method for analyzing fluid flow in porous media: Water Resour. Res., 12(1), p. 57-64.

Renner, J. L., D. E. White and D. L. Williams, 1975. Hydrothermal convection systems: U. S. Geol. Survey Circ. 726, p. 5-57.

Sorey, M. L., 1975. Numerical modeling of liquid geothermal systems: Ph.D. thesis, Univ. California, Berkeley, 65 p.

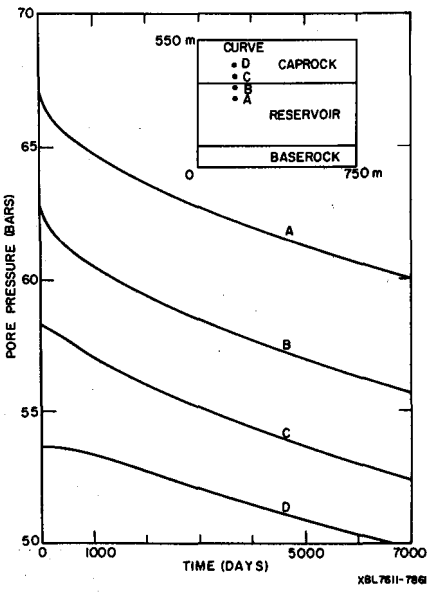

Figure 13. Example 4a. Pore pressure change with time at different points in the caprock and reservoir.

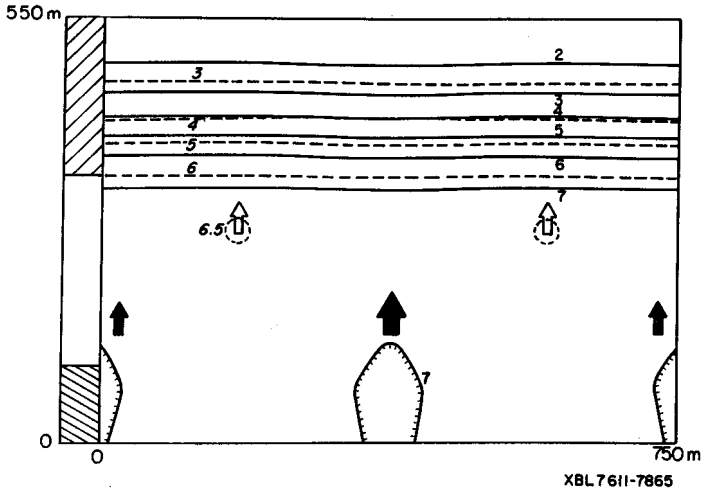

Figure 14. Example 4a. Pressure drop, in bars, after 20 years of simulation. Solid lines: non-isothermal case; Dashed lines: isothermal case; Dark arrows: injection; Light arrows: production (not to scale).

Stilwell, W. B., W. K. Hall and J. Tawhai, 1976. Ground movement in New Zealand geothermal fields: Proc. 2nd U. N. Symp. Development and Use of Geothermal Resources, San Francisco, Ca., May 20-29, 1975, p. 1427-1434.

Acknowledgement

This work was done with support from the U. S. Energy Research and Development Administration.

This report was done with support from the United States Energy Research and Development Administration. Any conclusions or opinions expressed in this report represent solely those of the author(s) and not necessarily those of The Regents of the University of California, the Lawrence Berkeley Laboratory or the United States Energy Research and Development Administration.